

# Nanoscale

Accepted Manuscript

This article can be cited before page numbers have been issued, to do this please use: T. Rollo, F. Blanchini, G. Giordano, R. Specogna and D. Esseni, *Nanoscale*, 2020, DOI: 10.1039/C9NR09470A.



This is an Accepted Manuscript, which has been through the Royal Society of Chemistry peer review process and has been accepted for publication.

Accepted Manuscripts are published online shortly after acceptance, before technical editing, formatting and proof reading. Using this free service, authors can make their results available to the community, in citable form, before we publish the edited article. We will replace this Accepted Manuscript with the edited and formatted Advance Article as soon as it is available.

You can find more information about Accepted Manuscripts in the [Information for Authors](#).

Please note that technical editing may introduce minor changes to the text and/or graphics, which may alter content. The journal's standard [Terms & Conditions](#) and the [Ethical guidelines](#) still apply. In no event shall the Royal Society of Chemistry be held responsible for any errors or omissions in this Accepted Manuscript or any consequences arising from the use of any information it contains.

# Stabilization of negative capacitance in ferroelectric capacitors with and without a metal interlayer

T. Rollo<sup>1</sup>, F. Blanchini<sup>2</sup>, G. Giordano<sup>3</sup>, R. Specogna<sup>1</sup>, D. Esseni<sup>1</sup>

<sup>1</sup>DPIA, University of Udine, Via delle Scienze 206, 33100 Udine, Italy; email: david.esseni@uniud.it

<sup>2</sup>DMIF, University of Udine, Via delle Scienze 206, 33100 Udine, Italy

<sup>3</sup>DII, University of Trento, via Sommarive 9, 38123 Povo (TN), Italy

## Abstract

The negative capacitance operation of a ferroelectric material is not only an intriguing material science topic, but also a property with important technological applications in nanoscale electron devices. Despite the growing interest for possible applications, the very existence of negative capacitance is still actively debated, even because experimental results for ferroelectric capacitors with or without a metal interlayer led to quite contradicting indications. Here we present a comprehensive analysis of the NC operation in ferroelectric capacitors and provide new insights about the discrepancies observed in experiments. Our models duly account for the three-dimensional nature of the problem and show a good agreement with several aspects of recent experiments. Our results also demonstrate that traps at the ferroelectric-dielectric interface play an important role in the feasibility of a stable negative capacitance operation in ferroelectric capacitors.

## 1 Introduction

The basic idea behind the use of ferroelectric materials in nanoscale transistors stems from the fact that, thanks to the negative capacitance (NC) operation, the voltage swing necessary to operate the transistors can be reduced,<sup>1–3</sup> thus enabling improved energy efficiency for CMOS circuits.<sup>4,5</sup> An industrial level demonstration of the NC operation in CMOS transistors was recently reported for a 14-nm FinFET technology,<sup>6</sup> with an analysis of the device and circuit level advantages further discussed in.<sup>7</sup> Moreover, several papers have started addressing diverse design aspects related to NC field effect transistors.<sup>8–10</sup>

Despite some encouraging experimental results, however, the stable NC operation of the ferroelectric is still quite controversial.<sup>11</sup> In fact, recent studies in Metal-Ferroelectric-Insulator-Metal (MFIM) capacitors reported a hysteresis free, direct measurement of the negative capacitance branch of a thin ferroelectric layer.<sup>12,13</sup> However, in similarly recent publications focused on Metal-Ferroelectric-Metal-Insulator-Metal (MFMIM) systems or on ferroelectric capacitors externally connected to a MOSFET authors either negated any evidence of the NC operation,<sup>14</sup> or affirmed that the measured steep slope transistor operation was due to domain switching and, as such, invariably accompanied by hysteresis.<sup>15–17</sup>

The discrepancy between experiments in MFIM and MFMIM systems is not entirely unexpected, in fact a recent theoretical investigation suggests that MFMIM capacitors are inherently more prone than MFIM systems to domain nucleation.<sup>18</sup> The analysis in,<sup>18</sup> however, was restricted to a one-dimensional, rigidly periodic system and, moreover, conclusions were drawn by inspecting the free energy landscapes, instead of examining the actual ferroelectric dynamic equations of the MFIM and MFMIM systems.

In this paper we present a comprehensive analysis of the dynamics and possible stabilisation of a ferroelectric layer inserted either in a MFIM or in a MFMIM structure, which is a broadly extended version of the concise contribution reported in.<sup>19</sup> To this purpose we have developed a model for the depolarisation energy that fully accounts for the three-dimensional nature of the electrostatics in a realistic device. Then we use the multi-domain Landau–Ginzburg–Devonshire theory (LGD) and derive analytical or quasi-analytical conditions for a stable NC operation, that explain the different behavior of a MFIM compared to a MFMIM capacitor. Our models are validated by a good agreement with several aspects of recent experiments.<sup>12,13</sup> Finally we investigate the influence of possible traps at the ferroelectric-dielectric interface, and argue that traps not only help explain some experimental features, but also discriminate between a quasi-static and a dynamic NC operation.

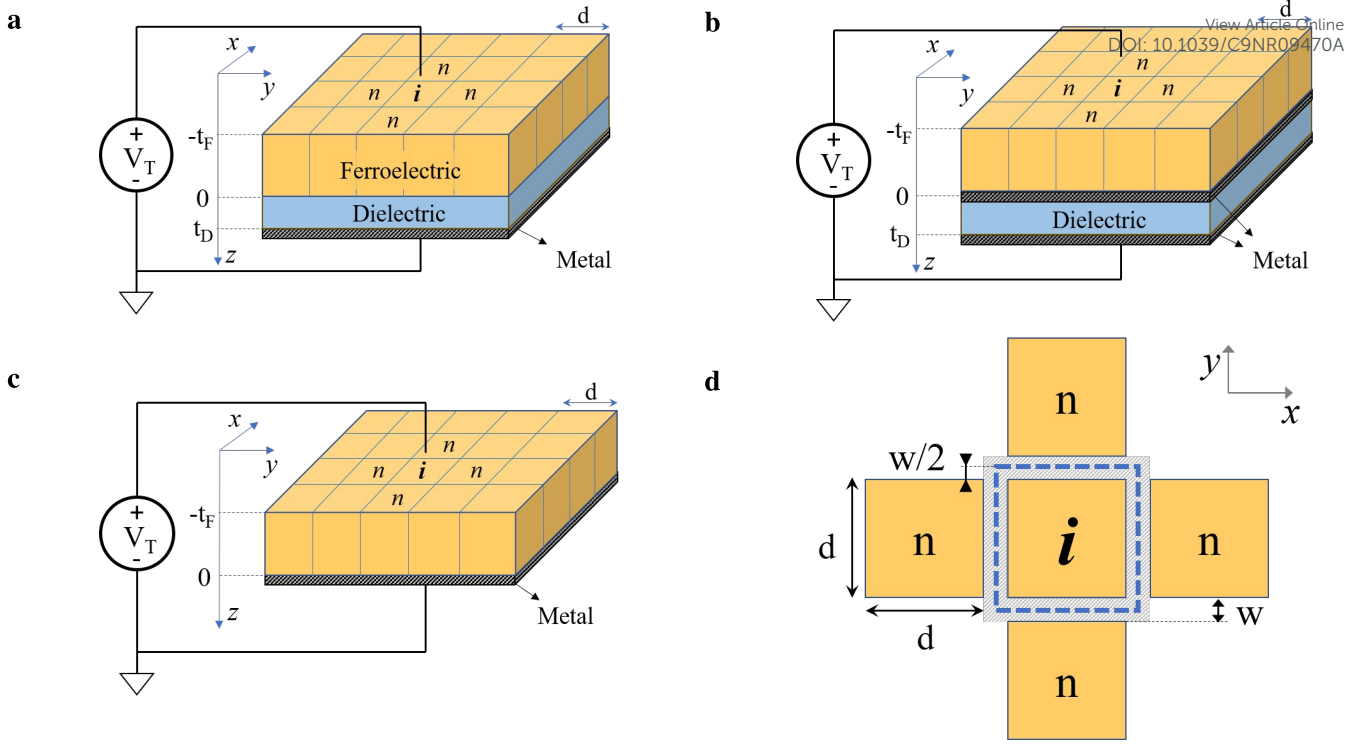


**Figure 1: Ferroelectric capacitors and related symbols.** **a.** Metal-Ferroelectric-Insulator-Metal (MFIM) and reference coordinate system. **b.** Metal-Ferroelectric-Metal-Insulator-Metal (MFIMIM) system. **c.** Metal-Ferroelectric-Metal (MFM) structure. The top metal contact is not shown for clarity.  $t_F$  and  $t_D$  denote respectively the ferroelectric and dielectric thickness,  $d$  is the domain side of a square domain of area  $d^2$ , and  $V_T$  is the externally applied voltage.  $V_D(\vec{r})$  is the electrostatic potential at the oxide interface (i.e. at  $z=0$ ), that depends on  $\vec{r}=(x,y)$  in a MFIM system, whereas it is independent of  $\vec{r}$  in a MFIMIM capacitor. **d.** Sketch of the ferroelectric domain  $i$  and its nearest neighbors domains  $n$  in the  $x$ - $y$  plane. The shaded area illustrates the domain-wall region, where  $w$  denotes the width, and the dashed blue line delimits the region used to compute the domain wall energy  $u_{w,i}$  in Eq.4.

## 2 Free energy and dynamic equations

In the analysis of the ferroelectric capacitors sketched in Fig.1 we assume that the spontaneous polarisation  $P$  lies along the  $z$  direction, and we write the free energy per unit volume of the ferroelectric by following<sup>18</sup>

$$u_F = \alpha P^2 + \beta P^4 + \gamma P^6 + k |\text{grad} P|^2 + \frac{\epsilon_0 \epsilon_F}{2} E_F^2 \quad (1)$$

where  $\alpha$ ,  $\beta$  and  $\gamma$  are the ferroelectric anisotropy constants,  $\epsilon_0$  is the vacuum permittivity,  $E_F$ ,  $\epsilon_F$  are respectively the electric field and relative background permittivity of the ferroelectric, while  $k$  is the coupling constant governing the domain wall energy and  $\text{grad} P$  denotes the gradient of  $P$ . The total polarisation in the ferroelectric is thus given by  $P_T = P + (\epsilon_F - 1)\epsilon_0 E_F$  and the electric displacement is  $D = P + \epsilon_F \epsilon_0 E_F$ .<sup>20</sup> We will assume that the ferroelectric has a second-order phase transition with  $\alpha < 0$ ,  $\beta > 0$ . When we consider the ferroelectric capacitors of Fig.1 the overall electrostatic energy consists of the three contributions<sup>21</sup>

$$\mathcal{U}_F = \frac{V_T}{2} \int_A \epsilon_0 \epsilon_F E_{F,T}(\vec{r}) d\vec{r}, \quad \mathcal{U}_B = -V_T \left[ d^2 \sum_{j=1}^{n_D} P_j + \int_A \epsilon_0 \epsilon_F E_{F,T}(\vec{r}) d\vec{r} \right], \quad \mathcal{U}_D = \sum_{j=1}^{n_D} \int_{D_j} \frac{P_j V_D(\vec{r})}{2} d\vec{r} \quad [J] \quad (2)$$

namely the ferroelectric self-energy,  $\mathcal{U}_F$ , the  $\mathcal{U}_B$  related to the external battery, and the electrostatic energy,  $\mathcal{U}_D$ , due to the dielectric region, which is zero in a MFM structure. Denoting by  $t_F$  the ferroelectric thickness,  $E_{F,T}(\vec{r}) = E_{F,z}(\vec{r}, -t_F)$  in Eq.2 is the electric field at the top metal interface and  $n_D$  is the number of domains. When we sum  $\mathcal{U}_F$ ,  $\mathcal{U}_B$ ,  $\mathcal{U}_D$  and normalise to the domain area  $d^2$  we obtain

$$U_{ET} = -\frac{V_T}{2} \frac{1}{d^2} \int_A \epsilon_0 \epsilon_F E_{F,T}(\vec{r}) d\vec{r} - V_T \sum_{j=1}^{n_D} P_j + \frac{1}{d^2} \sum_{j=1}^{n_D} \int_{D_j} \frac{P_j V_D(\vec{r})}{2} d\vec{r} \quad [J/m^2] \quad (3)$$

As for the domain wall energy, the polarisation is assumed to be essentially constant within each domain, so that  $\text{grad}P$  in Eq.1 is non null only in the domain wall region of Fig.1(d). The contribution  $u_{W,i}$  to the domain wall energy can thus be written as

$$u_{W,i} = \sum_n k \left( \frac{P_i - P_n}{w} \right)^2 \quad (4)$$

where  $w$  is the domain wall width shown in Fig.1(d), which we assume to be small enough to justify the discretized form of  $\text{grad}P$  in Eq.4 and, in particular, much smaller than  $d$ . We can now integrate  $u_{W,i}$  over the domain wall region inside the blue line in Fig.1(d) and along  $t_F$ , and then normalise to the domain area  $d^2$ , so as to obtain the domain wall energy per unit area

$$U_W = \sum_{j=1}^{n_D} \left[ \frac{t_F}{2d} \sum_n \frac{k}{w} (P_j - P_n)^2 \right] \quad [J/m^2] \quad (5)$$

The difference between the MFM, MFIM and MFMIM systems is in the  $U_{ET}$  defined in Eq.3. In the MFM case the last term in Eq.3 is zero and  $E_{F,T} = V_T/t_F$ , so that  $U_{ET} = -V_T \sum_{j=1}^{n_D} P_j - (n_D C_F V_T^2)/2$  with  $C_F = \epsilon_0 \epsilon_F / t_F$ . For the MFMIM structure the metal interlayer results in a one-dimensional electrostatics, so that  $E_{F,T}$  and  $V_D$  are independent of  $\bar{r}$  and given by  $E_{F,T} = (C_D V_T - P_{AV}) / (t_F C_0)$ ,  $V_D = (C_F V_T + P_{AV}) / C_0$ ,<sup>18</sup> where  $P_{AV} = (\sum_{j=1}^{n_D} P_j) / n_D$  is the average polarisation,  $C_D = \epsilon_0 \epsilon_D / t_D$  (where  $t_D$  denotes the dielectric thickness) and  $C_0 = (C_D + C_F)$ . For the MFIM system, instead, the calculation of the ferroelectric and dielectric field is a three-dimensional problem that demands a numerical evaluation. We show in Supplementary Section S1 that for both the MFMIM and the MFIM system the electrostatic energy reads

$$U_{ET} = U_{dep} - V_T \frac{C_D}{C_0} \sum_j^{n_D} P_j - \frac{C_S V_T^2}{2} n_D \quad (6)$$

where  $C_S = (C_F C_D) / (C_F + C_D)$ . Here  $U_{dep}$  denotes the depolarisation energy defined as

$$\text{MFMIM: } U_{dep} = \frac{n_D P_{AV}^2}{2C_0} \quad \text{MFIM: } U_{dep} = \frac{1}{2} \sum_{j,h=1}^{n_D} \frac{P_j P_h}{C_{j,h}} \quad (7)$$

where the capacitances  $C_{j,h}$  are defined in Eq.S4 of Supplementary Section S1, they obey the sum rules in Eq.S7, and all  $1/C_{j,h}$  tend to zero when  $t_D$  tends to zero. As it can be seen, the depolarisation energy  $U_{dep}$  vanishes when the dielectric thickness  $t_D$  tends to zero.

For all the systems in Fig.1 the overall free energy is  $U_T = \sum_{j=1}^{n_D} (\alpha P_j^2 + \beta P_j^4 + \gamma P_j^6) + U_W + U_{ET}$  and the corresponding dynamic equations read

$$\text{MFM: } t_F \rho \frac{dP_i}{dt} = - \frac{\partial U_T}{\partial P_i} = - \underbrace{(2\alpha P_i + 4\beta P_i^3 + 6\gamma P_i^5) t_F - \frac{t_F}{d} \sum_n \frac{k}{w} (P_i - P_n) + V_T(t)}_{= \partial U_{LGD}} \quad (8a)$$

$$\text{MFMIM: } t_F \rho \frac{dP_i}{dt} = \partial U_{LGD} - \frac{1}{n_D C_0} \sum_{j=1}^{n_D} P_j + \frac{C_D}{C_0} V_T(t) \quad (8b)$$

$$\text{MFIM: } t_F \rho \frac{dP_i}{dt} = \partial U_{LGD} - \frac{1}{2} \sum_{j=1}^{n_D} \left[ \frac{1}{C_{i,j}} + \frac{1}{C_{j,i}} \right] P_j + \frac{C_D}{C_0} V_T(t) \quad (8c)$$

where  $\rho$  is the resistivity governing the ferroelectric domain dynamics. It is straightforward to verify that, when the dielectric thickness  $t_D$  tends to zero,  $1/C_0$  and  $1/C_{i,j}$  tend to zero while  $[C_D/C_0]$  tends to one, so that Eq.8b and Eq.8c simplify to Eq.8a. Moreover for  $n_D=1$  Eq.8b and Eq.8c are identical, in fact the MFMIM and MFIM systems are equivalent, the domain wall energy is zero and Eq.8b, Eq.8c simplify to the well known single domain equation.<sup>18</sup>

### 3 Conditions for a stable NC operation

View Article Online

DOI: 10.1039/C9NR09470A

Throughout this paper we employ a definition of the NC operation consisting in the polarization  $P_i$  of all domains being zero at zero external voltage  $V_T$ , which ensures a hysteresis-free behavior also in the multi-domain picture. If the ferroelectric is stabilized in a region where  $P_i$  is not zero for most domains but  $\partial^2 G(P_i)/\partial^2 P_i$  is negative (with  $G(P_i) = (\alpha_i P_i^2 + \beta_i P_i^4 + \gamma_i P_i^6)$ ), an NC operation can still be claimed, albeit in the presence of hysteresis. The stable NC operation can be evaluated by inspecting the eigenvalues of the Jacobian matrices<sup>1</sup>,  $\mathbf{J}$ , of the dynamic systems in Eqs.8a, 8b and 8c evaluated for  $P_i=0$  in all domains. Here it should be noticed that analysing the stability of the equilibrium at  $P_i = 0$  and  $V_T=0$  is not restrictive. In fact, as we show in the Supplementary Section S4, stability in this case implies stability of the equilibrium for any other constant value of  $V_T$ . The Jacobian matrices read

$$\mathbf{J}_{MFM} = \frac{1}{\rho t_F} \left[ -2\alpha t_F \mathbf{I} - \frac{t_F k}{d w} \mathbf{L} \right] \quad (9a)$$

$$\mathbf{J}_{MFMIM} = \frac{1}{\rho t_F} \left[ -2\alpha t_F \mathbf{I} - \frac{t_F k}{d w} \mathbf{L} - \frac{\mathbf{O}_{dep}}{n_D C_0} \right] \quad (9b)$$

$$\mathbf{J}_{MFIM} = \frac{1}{\rho t_F} \left[ -2\alpha t_F \mathbf{I} - \frac{t_F k}{d w} \mathbf{L} - \mathbf{C}_{dep} \right] \quad (9c)$$

where  $\mathbf{I}$  is the  $n_D$  by  $n_D$  identity matrix, while  $\mathbf{L}$  is the Laplacian matrix<sup>2</sup>. The matrix  $\mathbf{O}_{dep}$  has all entries equal to one, whereas  $\mathbf{C}_{dep}$  is defined as

$$C_{dep}(i, j) = \frac{1}{2} \left[ \frac{1}{C_{i,j}} + \frac{1}{C_{j,i}} \right] \quad (10)$$

The matrices  $\mathbf{O}_{dep}$  and  $\mathbf{C}_{dep}$  stem from the depolarisation energy  $U_{dep}$  in Eq.7, and are very different for a MFMIM and a MFIM system. The eigenvalues of the symmetric  $\mathbf{J}$  matrices in Eq.9 are real valued and, for a stable NC operation, it is required that the largest eigenvalue  $\sigma_{max}(\mathbf{J})$  of the Jacobian matrix evaluated for all  $P_i=0$  be negative.<sup>22</sup> This results in the equivalent stability conditions

$$\text{MFM:} \quad \frac{k}{d w} \sigma_{min}(\mathbf{L}) > 2|\alpha| \quad (11a)$$

$$\text{MFMIM:} \quad \sigma_{min} \left[ \frac{t_F k}{d w} \mathbf{L} + \frac{\mathbf{O}_{dep}}{n_D C_0} \right] > 2|\alpha| t_F \quad (11b)$$

$$\text{MFIM:} \quad \sigma_{min} \left[ \frac{t_F k}{d w} \mathbf{L} + \mathbf{C}_{dep} \right] > 2|\alpha| t_F \quad (11c)$$

where  $\sigma_{min}(\mathbf{M})$  denotes the smallest eigenvalue of the matrix  $\mathbf{M}$ .

We now recall that the eigenvalues of  $\mathbf{L}$  are known analytically in our case (since we are dealing with a rectangular grid) and the smallest and second smallest eigenvalue are  $\sigma_0(\mathbf{L})=0$  and  $\sigma_1(\mathbf{L})=[2\sin(\pi/(2\sqrt{n_D}))]^2$ .<sup>23</sup> This implies that, as expected, the MFM system is always unstable for all  $P_i=0$ .

For the MFMIM system we show in Supplementary Section S2 that, due to the peculiar form of the matrix  $\mathbf{O}_{dep}$ , one can derive the analytical (necessary and sufficient) condition for a stable NC operation given by

$$\min \left\{ \frac{1}{C_0}, \frac{t_F k}{d w} [2 \sin(\pi/(2\sqrt{n_D}))]^2 \right\} > 2|\alpha| t_F \quad (12)$$

Eq.12 shows that in the MFMIM system the effect of the depolarisation energy is very limited, in fact  $\mathbf{O}_{dep}$  can only eliminate the influence of  $\sigma_0(\mathbf{L})=0$  but not the influence of  $\sigma_1(\mathbf{L})$ . Eq.12 also affirms that the condition  $(1/C_0) > 2|\alpha| t_F$  is necessary for the stability of the MFMIM system. Moreover, for a relatively large number of domains such that  $\sin(\pi/(2\sqrt{n_D})) \simeq \pi/(2\sqrt{n_D})$ , Eq.12 suggests that a stable NC operation for the MFMIM system requires  $k/w$  values that increase proportionally to  $n_D$ , hence to the device area.

<sup>1</sup>The Jacobian matrix of the system of dynamic equations  $dP_i/dt = f_i(P_1, \dots, P_{n_D})$  is defined component-wise as  $J(i, j) = \partial f_i / \partial P_j$ .

<sup>2</sup> $\mathbf{L}$  is defined component-wise as  $\mathbf{L}(i, j) = -1$  if domain  $j$  is a neighbour of domain  $i$  and  $\mathbf{L}(i, j) = 0$  otherwise (see Fig.1(d)), and  $\mathbf{L}(i, i) = -\sum_{j \neq i} \mathbf{L}(i, j)$ .

For the MFIM structure it is not possible to derive analytical eigenvalues and stability conditions from Eq. 11c, but a numerical analysis shows that  $\mathbf{C}_{dep}$  has a much larger influence on NC stabilisation than  $\mathbf{C}_{dep}$  for the MFIM system. Moreover we show in Supplementary Section S3 that even for the MFIM system the inequality  $(1/C_0) > 2|\alpha|_{t_F}$  is still a necessary condition for a stable NC operation. It is interesting to notice that this is the stability condition previously derived for a single domain system.<sup>18</sup>

Ferroelectric materials may have domain to domain statistical variations of the ferroelectric anisotropy constants, whose influence on the stable NC operation is addressed in Supplementary Section S5.

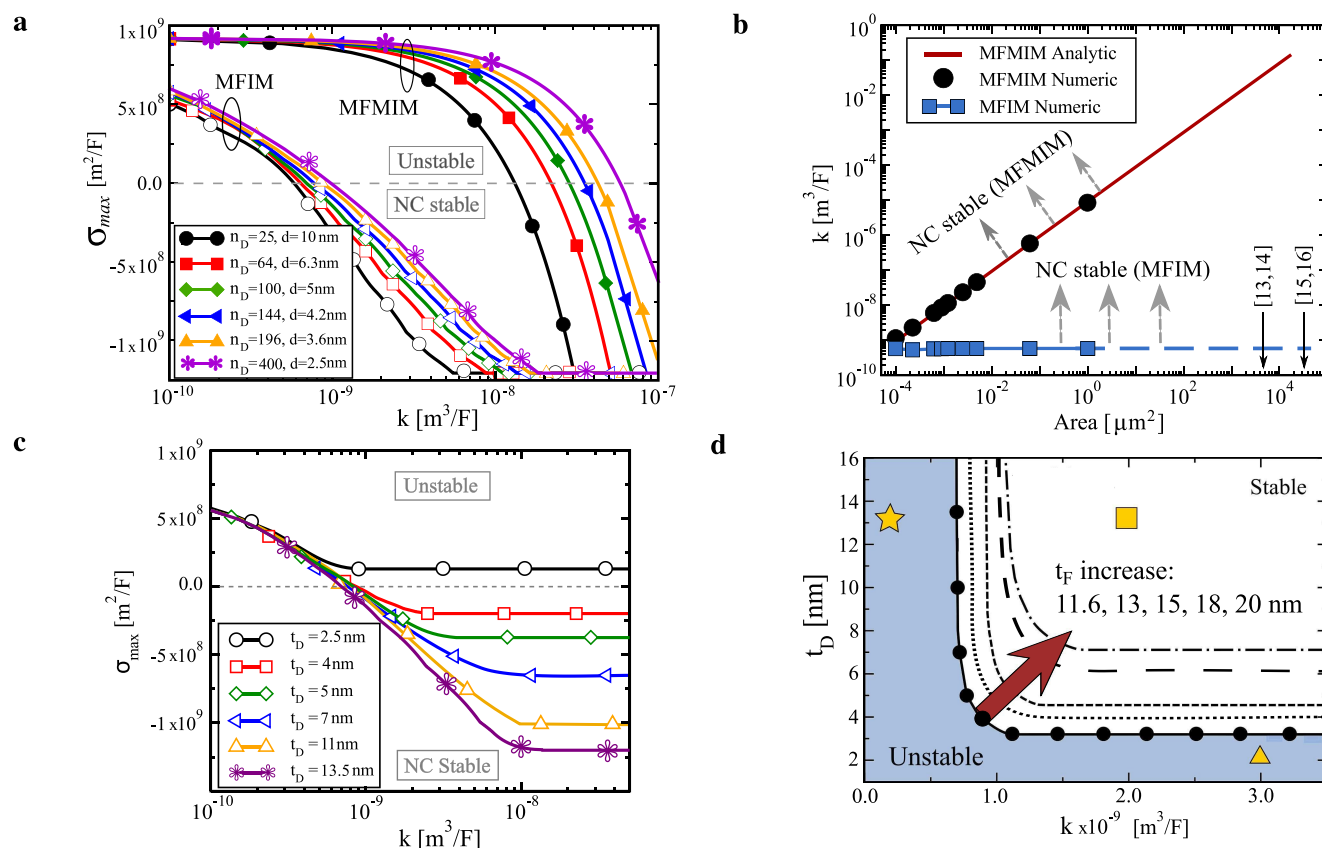


**Figure 2: Eigenvalues of the Jacobian matrix and design space for stable NC operation:** **a.** Largest eigenvalue  $\sigma_{max}$  of the Jacobian matrix for all  $P_i=0$  versus the domain wall coupling factor  $k$  for either a MFIM (numerically calculated) or a MFMIM structure. Capacitor area is  $A=2500\text{nm}^2$  and results are shown for different combinations of  $d$  and  $n_D$ . Stable NC operation corresponds to  $\sigma_{max} < 0$ . **b.** Minimum coupling factor  $k$  necessary for a stable NC operation versus the capacitor area for either a MFMIM or a MFIM structure. For the MFIM structure results have been calculated numerically from the condition  $\sigma_{max} < 0$ , while for the MFMIM structure results stem from Eq.12. Domain size is  $d=5\text{nm}$ , thus  $\text{Area}=d^2 n_D$ . Please notice the large areas corresponding to recent experiments in.<sup>13-16</sup> **c.** Maximum eigenvalue  $\sigma$  versus coupling factor  $k$  obtained from numerical simulations for a MFIM structure having different  $\text{Ta}_2\text{O}_5$  thicknesses  $t_D$ . Ferroelectric thickness, domain number  $n_D$  and domain area  $d^2$  area set to  $t_F=11.6\text{nm}$ ,  $n_D=100$  and  $d^2=25\text{nm}^2$ . **d.** Regions for stable NC operation for a MFIM structure in the  $t_D$  versus  $k$  plane and for different  $t_F$  values. Filled circles correspond to  $t_F=11.6\text{nm}$ . For larger  $t_F$  values the minimum  $t_D$  required for stability increases, as predicted by the necessary condition  $(1/C_0) > 2|\alpha|t_F$ . Area is  $A=2500\text{nm}^2$  and  $n_D=100$ . The star, square and triangle symbols identify the  $t_D$  and  $k$  values corresponding to some of the simulations in Fig.3, and are discussed in the text.

## 4 Physical insight and design space

All the simulation results reported in this work were obtained for  $\epsilon_F=33$ ,  $\epsilon_D=23.5$ ,  $t_F=11.6$  nm,  $t_D=13.5$  nm,  $\alpha=-4.6\cdot 10^8$  m/F,  $\beta=9.8\cdot 10^9$  m<sup>5</sup>/C<sup>2</sup>/F and  $\gamma=0$ , if not otherwise stated, namely the material parameters that have been reported for the Hf<sub>0.5</sub>Zr<sub>0.5</sub>O<sub>2</sub>-Ta<sub>2</sub>O<sub>5</sub> MFIM system in.<sup>13</sup>

Fig.2(a) reports the maximum eigenvalue  $\sigma_{max}$  of the Jacobian for all  $P_i=0$  versus the coupling factor  $k$  for either MFMM or MFIM structures with an area  $A=2500\text{nm}^2$ , and for different combinations of  $n_D$  and  $d$ . As it can be seen the MFIM capacitor can achieve NC stabilisation for smaller  $k$  values compared to the MFMM system, and it has a much weaker sensitivity to the increase of  $n_D$ . The substantial difference in the NC stabilisation of

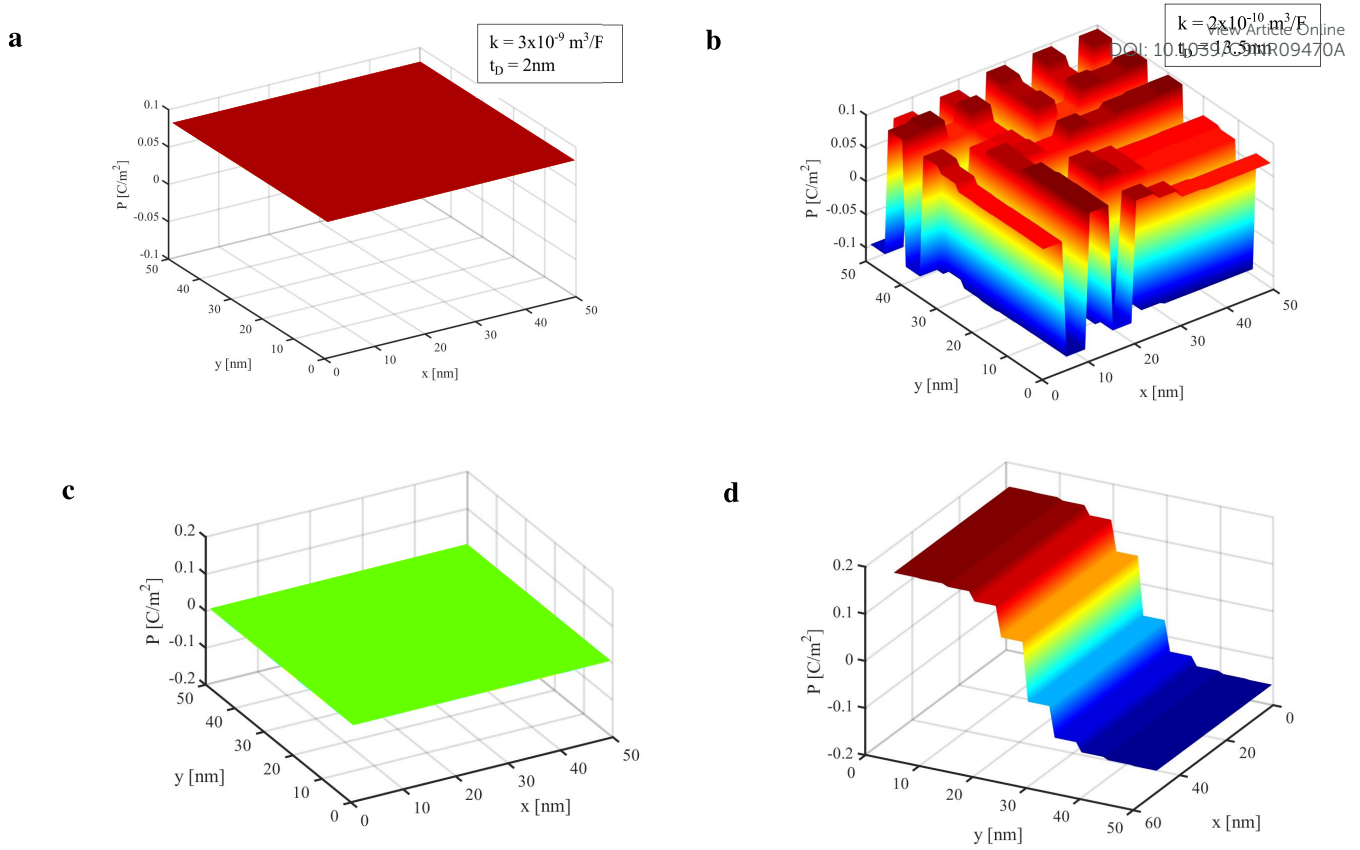


**Figure 3: Ferroelectric domain patterns for MFIM and MFMIM capacitors.** Steady-state domain configuration at  $V_T=0V$ . **a.** MFIM system: small  $t_D$  and high  $k$  value that do *not* correspond to a stable NC operation, see triangle in Fig.2(b). **b.** MFIM system: large  $t_D$  and small  $k$  value that do *not* correspond to a stable NC operation, see star in Fig.2(b). **c.** MFIM system with  $t_D=13.5\text{nm}$ ,  $t_F=11.6\text{nm}$  and  $k=2 \times 10^{-9} \text{ m}^3/\text{F}$ , which correspond to a stable NC operation, see square in Fig.2(b). **d.** MFMIM capacitor having the same material and device parameters as the MFIM in **c**.

MFIM and MFMIM systems for large  $n_D$  is better illustrated by Fig.2(b), showing that for the MFMIM system the  $k$  value required for NC stabilisation increases proportionally to  $n_D$  and thus to the device areas. This makes NC stabilisation practically impossible for MFMIM systems having areas as those used in recent experiments.<sup>14–16</sup>

Fig.2(c)(d) focus on the MFIM system and report respectively the numerically calculated  $\sigma_{max}$  of the Jacobian matrix (for all  $P_i=0$ ) for different  $t_D$  and at fixed  $t_F$ , and the design regions for a stable NC operation of a MFIM structure in the  $t_D-k$  plane and for  $n_D=100$ . As it can be seen the NC operation is not possible for too thin oxides, because the necessary condition  $(1/C_0) > 2|\alpha|t_F$  is not fulfilled and, for any  $t_D$  satisfying the above condition, we have a minimum  $k$  value necessary for stabilisation. For  $t_D$  larger than about 10 nm the  $k$  for NC stabilisation becomes independent of  $t_D$ . This occurs because, while at small  $t_D$  the potential  $V_D$  at the ferroelectric-dielectric interface and the depolarisation energy  $U_{dep}$  decrease by scaling  $t_D$ , at large  $t_D$  the  $U_{dep}$  becomes insensitive to  $t_D$ .

According to the empirical formula for the NC stable operation of a one-dimensional and periodic MFIM system proposed in Eq.15 of,<sup>18</sup> the  $t_D$  independent  $k$  value necessary for NC operation is  $k = 1.2 \cdot 10^9 [\text{m}^3/\text{F}]$  for  $t_F=11.6 \text{ nm}$ , and  $k = 2.1 \cdot 10^9 [\text{m}^3/\text{F}]$  for  $t_F=20 \text{ nm}$ . These  $k$  values are about two times larger than the values in Fig.2(d) obtained for the two-dimensional ferroelectric domain arrangement studied in this work. In more general terms we found that, while the qualitative trends obtained from our 3D analysis are similar to those predicted by the Eq.15 of,<sup>18</sup> the regions for NC stabilization identified by our results are larger. For example our 3D results suggest that, for a given couple  $(t_D, t_F)$ , a smaller  $k$  is sufficient for stabilization and, for a given  $(t_D, k)$ , the system is NC stable up to larger  $t_F$  values.

While Fig.2 illustrates the design space for a stable NC operation, it is also insightful to inspect the steady-state configuration of domains obtained by solving the LGD dynamic equations. In this respect, Fig.3(a) reports the steady-state domain configuration at  $V_T=0$  for a MFIM system corresponding to the triangle symbol in Fig.2(d), namely to a system where the condition  $(1/C_0) > 2|\alpha|t_F$  necessary for NC stabilisation is not fulfilled. As it

can be seen the MFIM evolves so as to minimise the domain wall energy, whose minimum value is achieved by having all the domains with a positive polarisation. This steady-state polarisation pattern resembles the pattern of a MFM system, which the MFIM capacitor in fact approximates when  $t_D$  and  $U_{dep}$  become very small. Fig.3(b), instead, illustrates the case corresponding to the star symbol in Fig.2(d), namely to a system where the condition  $(1/C_0) > 2|\alpha|t_F$  is fulfilled, but the domain wall constant  $k$  is too small for the NC stabilisation. In this case the system tends to minimise the depolarisation energy by having domains with different polarisations, even if this implies a larger domain wall energy compared to the pattern in Fig.3(a). Fig.3(c),(d) illustrate the steady-state domain configuration at  $V_T=0$  for a MFIM with  $k=2 \cdot 10^{-9} \text{ m}^3/\text{F}$  (square symbol in Fig.2(d)), and for the counterpart MFMIM. Consistently with Fig.2(d), the steady-state condition for the MFIM system corresponds to all  $P_i=0$ . The MFMIM, instead, is not stable for all  $P_i=0$ , and therefore it evolves to a configuration corresponding to  $P_{AV}=(\sum_{i=1}^{n_D} P_i)/n_D \simeq 0$ .

Fig.3(c) and (d) demonstrate that the crucial difference between MFMIM and MFIM systems is that the depolarisation energy of the MFMIM system at  $V_T=0$  is zero if  $P_{AV}$  is zero (see Eq.7). Hence if the MFMIM is initialised with all  $P_i=0$ , it gets destabilised along trajectories having  $P_{AV} \simeq 0$  and thus  $U_{dep} \simeq 0$ , which is confirmed by the steady-state configuration in Fig.3(d). The same trajectories are precluded in the MFIM system because the corresponding  $U_{dep}$  in Eq.7 is not at all zero, hence it is the form of the  $U_{dep}$  which makes the NC stabilisation possible in MFIM capacitors.

The analysis developed in this paper and the results presented in this section assumed that the leakage current through the oxides is small enough to not influence the NC stabilization. As already recognized in,<sup>24,25</sup> in a MFMIM structure the presence of a non negligible leakage essentially precludes the NC stabilization.

## 5 Comparison with experimental results

As a validation of our modelling approach we now illustrate a systematic comparison with recent experiments reported for an  $\text{Hf}_{0.5}\text{Zr}_{0.5}\text{O}_2$  based MFIM structure.<sup>12,13</sup> The simulations account for the presence of a fixed charge  $Q_{DF}=0.15 \text{ C/cm}^2$  at the interface between  $\text{Hf}_{0.5}\text{Zr}_{0.5}\text{O}_2$  and  $\text{Ta}_2\text{O}_5$ , which results in the fact that the ferroelectric is biased in the negative polarisation branch for  $V_T=0 \text{ V}$ .<sup>12</sup> Simulations correspond to a domain size of  $d=5 \text{ nm}$  and a domain number  $n_D=100$ , and we verified that results are insensitive to any further  $n_D$  increase. The pulse width of the trapezoidal input waveform  $V_T(t)$  is set to  $1 \mu\text{s}$  (if not otherwise stated), which is small enough to make the ferroelectric time constants practically negligible for the small resistivity value  $\rho=0.5 \text{ m}\Omega\cdot\text{m}$  employed in these simulations.

Fig.4(a) reports the charge  $Q=P+\epsilon_F\epsilon_0 E_F+Q_{DF}$  versus the top value  $V_{max}$  of the trapezoidal voltage waveform applied across the  $\text{Hf}_{0.5}\text{Zr}_{0.5}\text{O}_2\text{--Ta}_2\text{O}_5$  capacitor, and shows a good agreement between simulations and experiments. Fig.4(b) illustrates the simulated waveforms for the ferroelectric field,  $E_F$ , and the total ferroelectric polarization,  $P_T=P+\epsilon_F\epsilon_0 E_F$ , produced by trapezoidal input  $V_T$  and for three  $V_T$  amplitudes. By using the  $E_F$  and  $P_T$  values observed in Fig.4(b), we obtained the charge versus ferroelectric field curves reported in Fig.4(c)(d) respectively for the  $\text{Hf}_{0.5}\text{Zr}_{0.5}\text{O}_2\text{--Ta}_2\text{O}_5$  and  $\text{Hf}_{0.5}\text{Zr}_{0.5}\text{O}_2\text{--Al}_2\text{O}_3$  capacitor. As it can be seen simulations nicely reproduce the fact that, for the experimental conditions at study, the ferroelectric layer can be operated in the NC operation region, which is the physical origin of the change of slope in the  $Q$  versus  $V_{max}$  plot of Fig.4(b). We also verified that, as long as the NC stabilization is guaranteed, different  $t_D$  values still result in the same  $P_T$  versus  $E_F$  curves for the quasi-static NC operation explored in this work.

From the charge versus  $V_T$  plots as in Fig.4(a) we numerically calculated the capacitance  $C_T=(\partial Q/\partial V_T)$  in the NC stabilized region and compared to results the simple analytical expression  $C_T=C_D \cdot [|C_{F,0}|/(|C_{F,0}| - C_D)]$ , with  $C_{F,0}=[1/(2\alpha t_F)+\epsilon_F/t_F]$  being the zero field ferroelectric capacitance. This analysis showed that, while the numerically calculated  $C_T$  is quite bias dependent even inside the NC region, the analytical expression is in very close agreement with the maximum  $C_T$ . Because the term  $[|C_{F,0}|/(|C_{F,0}| - C_D)]$  can be seen as an enhancement factor of  $C_T$  with respect to  $C_D$ , the analytical expression allows one to easily estimate the capacitance enhancement from the dielectric and ferroelectric parameters  $\epsilon_D$ ,  $t_D$ ,  $\alpha$ ,  $\epsilon_F$ ,  $t_F$ .

We also developed a model to study the influence of traps at the ferroelectric-dielectric interface, according to a simple kinetic equation for the trap occupation that we solved self-consistently with the LGD equations, as discussed in detail in the Supplementary Section S6. Fig.4(e) illustrates that traps are assumed to exchange electrons via tunneling with the bottom metal contact. While the bias independent rate  $e_{n0}$  could be described

by models similar to those used for border traps in MOS transistors,<sup>26,27</sup> such a quantitative description of the emission rates goes beyond the scope of the present work, where we investigate only the qualitative features induced by traps and, to this purpose, we consider  $e_{n0}$  as a free parameter in the comparison to experiments. In this respect, Fig.4(f) illustrates experiments and simulations for the charge versus ferroelectric field obtained for different pulse widths of the trapezoidal input waveform, where simulations correspond to a uniform density  $N_T=7.5 \times 10^{12} \text{ eV}^{-1}\text{cm}^{-2}$  of acceptor type traps. As it can be seen, by using  $e_{n0}=5.0 \cdot 10^4 \text{ s}^{-1}$  the simulations can reproduce quite well the influence of the pulse width on the  $Q$  versus  $E_F$  curves observed in experiments. The influence of traps on the stability conditions of a MFIM system is further addressed in the Supplementary Section S6.

In summary, we presented a methodology to investigate a possible stable NC operation in ferroelectric capacitors based on the LGD dynamic equations and duly accounting for the three-dimensional nature of the problem. From the Jacobian matrix of the LGD equations we derived analytical or semi-analytical stability conditions, that clarified important differences between a MFIM and a MFMIM system. Our analysis is consistent with the fact that a stable NC operation has been observed in MFIM systems but not in MFMIM systems, and suggests MFMIM capacitors or capacitors externally connected to a MOSFET are inherently unsuitable to study the stable NC operation.

A systematic comparison with recent experiments in MFIM capacitors provides convincing evidence that the NC operation of the ferroelectric  $\text{Hf}_{0.5}\text{Zr}_{0.5}\text{O}_2$  can nicely explain experimental data. The critical role of interface traps emphasizes the importance of the quality of the ferroelectric-dielectric interface in the NC operation of ferroelectric capacitors and transistors.

We conclude by remarking that, while in a robustly NC stabilized system domains tend to move together thus resulting in a fairly 1D electrostatics, we verified that the electrostatics becomes strongly 3D when domain nucleation occurs and the system becomes hysteretic. The methodology for the dynamics of ferroelectric domain developed in this paper is thus expected to be important also for the analysis of a transient and possibly hysteretic NC operation, as well as for the investigation of Ferroelectric Tunnelling Junctions to be used either as non volatile memories or as memristors for neuromorphic computing applications.<sup>28</sup>

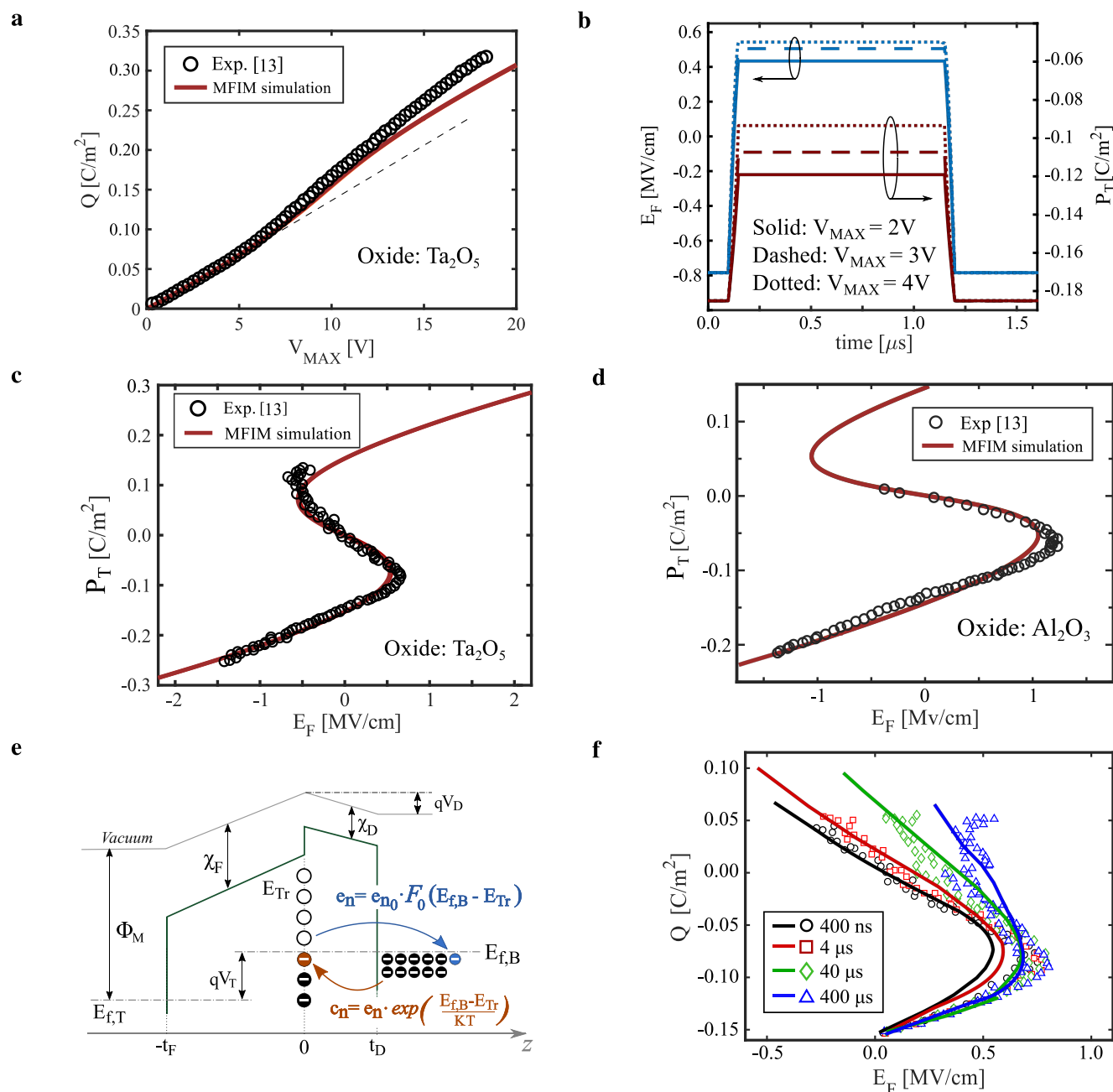


**Figure 4: Comparison between simulations and experiments.** Measurements (symbols) and simulations (lines) for the MFIM structures in.<sup>12,13</sup> For the  $\text{Hf}_{0.5}\text{Zr}_{0.5}\text{O}_2\text{-Ta}_2\text{O}_5$  capacitor the simulation parameters are  $\epsilon_F=33$ ,  $\epsilon_D=23.48$ ,  $t_F=11.6\text{nm}$ ,  $t_D=13.5\text{nm}$ ,  $\alpha=-4.6 \cdot 10^8\text{m/F}$ ,  $\beta=9.8 \cdot 10^9\text{m}^5/\text{C}^2/\text{F}$ , while for the  $\text{Hf}_{0.5}\text{Zr}_{0.5}\text{O}_2\text{-Al}_2\text{O}_3$  system the parameters are  $\epsilon_D=8$ ,  $t_F=7.7\text{nm}$ ,  $t_D=4\text{nm}$ ,  $\alpha=-9.45 \cdot 10^8\text{m/F}$  and  $\beta=2.25 \cdot 10^{10}\text{m}^5/\text{C}^2/\text{F}$ .<sup>12,13</sup> for both capacitors we used  $\rho=0.5\text{m}\Omega\cdot\text{m}$  and  $k=2 \cdot 10^{-9}\text{m}^3/\text{F m}$ . **a.** Reversibly stored and released charge,  $Q$ , versus the top value  $V_{\text{MAX}}$  of the trapezoidal voltage waveform across the capacitor. **b.** Simulated ferroelectric field and charge versus time produced by a trapezoidal input  $V_T$  with a pulse width of  $1\mu\text{s}$  and for different  $V_T$  amplitudes. **c.** Polarisation versus ferroelectric electric field for the  $\text{Hf}_{0.5}\text{Zr}_{0.5}\text{O}_2\text{-Ta}_2\text{O}_5$  MFIM capacitor. **d.** Polarisation versus ferroelectric electric field for the  $\text{Hf}_{0.5}\text{Zr}_{0.5}\text{O}_2\text{-Al}_2\text{O}_3$  capacitor. **e.** Sketch of the band structure of the MFIM device with representation of the emission and capture mechanisms. **f.** Simulated charge versus ferroelectric  $E_F$  curves for different pulse widths of the input signal and fixed density  $N_T=7.5^{12}\text{eV}^{-1}\text{cm}^{-2}$  of acceptor type interface traps with a uniform energy distribution. In these simulations the emission rate is  $e_{n0}=5 \times 10^4\text{s}^{-1}$ , the metal gate work-function is  $\Phi_M=4.05\text{eV}$ , and the electron affinity is  $\chi_F=2.2\text{eV}$  for  $\text{Hf}_{0.5}\text{Zr}_{0.5}\text{O}_2$  and  $\chi_D=3.2\text{eV}$  for  $\text{Ta}_2\text{O}_5$ .<sup>29</sup>

## References

View Article Online  
DOI: 10.1039/C9NR09470A

- <sup>1</sup> S. Salahuddin and S. Datta, "Use of Negative Capacitance to Provide Voltage Amplification for Low Power Nanoscale Devices," *Nano Letters*, vol. 8, no. 2, 2008. doi: 10.1021/nl071804g
- <sup>2</sup> A. I. Khan, "On the Microscopic Origin of Negative Capacitance in Ferroelectric Materials: A Toy Model," in *2018 IEEE International Electron Devices Meeting (IEDM)*, 2018. doi: 10.1109/IEDM.2018.8614574. ISSN 2156-017X pp. 9.3.1–9.3.4.
- <sup>3</sup> J. C. Wong and S. Salahuddin, "Negative Capacitance Transistors," *Proceedings of the IEEE*, vol. 107, no. 1, pp. 49–62, 2019.
- <sup>4</sup> T. N. Theis and P. M. Solomon, "In Quest of the Next Switch: Prospects for Greatly Reduced Power Dissipation in a Successor to the Silicon Field-Effect Transistor," *Proceedings of the IEEE*, vol. 98, no. 12, pp. 2005–2014, 2010.
- <sup>5</sup> A. C. Seabaugh and Q. Zhang, "Low-Voltage Tunnel Transistors for Beyond CMOS Logic," *Proceedings of the IEEE*, vol. 98, no. 12, pp. 2095–2110, 2010. doi: 10.1109/JPROC.2010.2070470
- <sup>6</sup> Z. Krivokapic, U. Rana, R. Galatage, A. Razavieh, A. Aziz, J. Liu, J. Shi, H. Kim, R. Sporer, C. Serrao, A. Busquet, P. Polakowski, J. Mülle, W. Kleemeier, A. Jacob, D. Brown, A. Knorr, R. Carter, and S. Banna, GLOBALFOUNDRIES, "14nm Ferroelectric FinFET Technology with Steep Subthreshold Slope for Ultra Low Power Applications," in *2017 IEEE International Electron Devices Meeting (IEDM)*, 2017. doi: 10.1109/IEDM.2017.8268393. ISSN 2156-017X pp. 357–360.
- <sup>7</sup> D. Kwon, Y. Liao, Y. Lin, J. P. Duarte, K. Chatterjee, A. J. Tan, A. K. Yadav, C. Hu, Z. Krivokapic, and S. Salahuddin, "Response Speed of Negative Capacitance FinFETs," in *2018 IEEE Symposium on VLSI Technology*, 2018. doi: 10.1109/VLSIT.2018.8510626. ISSN 2158-9682 pp. 49–50.
- <sup>8</sup> T. Rollo and D. Esseni, "Energy Minimization and Kirchhoff's Laws in Negative Capacitance Ferroelectric Capacitors and MOSFETs," *IEEE Electron Device Letters*, vol. 38, no. 6, pp. 814–817, 2017. doi: 10.1109/LED.2017.2691002
- <sup>9</sup> T. Rollo and D. Esseni, "New Design Perspective for Ferroelectric NC-FETs," *IEEE Electron Device Letters*, vol. 39, no. 4, pp. 603–606, 2018. doi: 10.1109/LED.2018.2795026
- <sup>10</sup> T. Rollo and D. Esseni, "Influence of Interface Traps on Ferroelectric NC-FETs," *IEEE Electron Device Letters*, vol. 39, no. 7, pp. 1100–1103, 2018. doi: 10.1109/LED.2018.2842087
- <sup>11</sup> M. A. Alam, M. Si, and P. D. Ye, "A critical review of recent progress on negative capacitance field-effect transistors," *Applied Physics Letters*, vol. 114, no. 9, p. 090401, 2019. doi: 10.1063/1.5092684. [Online]. Available: <https://doi.org/10.1063/1.5092684>
- <sup>12</sup> M. Hoffmann, B. Max, T. Mittmann, U. Schroeder, S. Slesazeck, and T. Mikolajick, "Demonstration of High-speed Hysteresis-free Negative Capacitance in Ferroelectric  $Hf_{0.5}Zr_{0.5}O_2$ ," in *2018 IEEE International Electron Devices Meeting (IEDM)*, 2018. doi: 10.1109/IEDM.2018.8614677. ISSN 2156-017X pp. 31.6.1–31.6.4.
- <sup>13</sup> M. Hoffmann, F. P. G. Fengler, M. Herzig, T. Mittmann, B. Max, U. Schroeder, R. Negrea, P. Lucian, S. Slesazeck, and T. Mikolajick, "Unveiling the double-well energy landscape in a ferroelectric layer," *Nature*, vol. 565, pp. 464–467, 2019. doi: 10.1038/s41586-018-0854-z. [Online]. Available: <https://doi.org/10.1038/s41586-018-0854-z>
- <sup>14</sup> Z. Liu, M. A. Bhuiyan, and T. P. Ma, "A Critical Examination of 'Quasi-Static Negative Capacitance' (QSNC) theory," in *2018 IEEE International Electron Devices Meeting (IEDM)*, 2018. doi: 10.1109/IEDM.2018.8614614. ISSN 2156-017X pp. 31.2.1–31.2.4.
- <sup>15</sup> X. Li and A. Toriumi, "Direct relationship between sub-60 mV/dec subthreshold swing and internal potential instability in MOSFET externally connected to ferroelectric capacitor," in *2018 IEEE International Electron Devices Meeting (IEDM)*, 2018. ISSN 2156-017X pp. 31.3.1–31.3.4.

- <sup>16</sup> H. Wang, M. Yang, Q. Huang, K. Zhu, Y. Zhao, Z. Liang, C. Chen, Z. Wang, Y. Zhong, X. Zhang, and R. Huang, "New Insights into the Physical Origin of Negative Capacitance and Hysteresis in NCFETs," in *2018 IEEE International Electron Devices Meeting (IEDM)*, 2018. doi: 10.1109/IEDM.2018.8614504. ISSN 2156-017X pp. 31.1.1–31.1.4.
- <sup>17</sup> J. Van Houdt and P. Roussel, "Physical Model for the Steep Subthreshold Slope in Ferroelectric FETs," *IEEE Electron Device Letters*, vol. 39, no. 6, pp. 877–880, 2018. doi: 10.1109/LED.2018.2829604
- <sup>18</sup> M. Hoffmann, M. Pešić, S. Slesazeck, U. Schroeder, and T. Mikolajick, "On the stabilization of ferroelectric negative capacitance in nanoscale devices," *Nanoscale*, vol. 10, pp. 10 891–10 899, 2018. doi: 10.1039/C8NR02752H. [Online]. Available: <http://dx.doi.org/10.1039/C8NR02752H>
- <sup>19</sup> T. Rollo, F. Blanchini, G. Giordano, R. Specogna, and D. Esseni, "Revised analysis of negative capacitance in ferroelectric-insulator capacitors: analytical and numerical results, physical insight, comparison to experiments," in *2019 IEEE International Electron Devices Meeting (IEDM)*, 2019, pp. 7.2.1–7.2.4.
- <sup>20</sup> C. H. Woo and Y. Zheng, "Depolarization in modeling nano-scale ferroelectrics using the Landau free energy functional," *Applied Physics A*, p. 59–63, 2008. doi: 10.1007/s00339-007-4355-4
- <sup>21</sup> E. M. Purcell, *Electricity and Magnetism*. Oxford University, 2013. ISBN 0-89871-465-6
- <sup>22</sup> D. G. Luenberger, *Introduction To Dynamic Systems*. John Wiley & Sons, 1979. ISBN 10:0471025941
- <sup>23</sup> M. Fiedler, "Algebraic connectivity of graphs," *Czechoslovak Mathematical Journal*, vol. 23, no. 2, pp. 298–305, 1973. [Online]. Available: <http://eudml.org/doc/12723>
- <sup>24</sup> A. I. Khan, U. Radhakrishna, S. Salahuddin, and D. Antoniadis, "Work function engineering for performance improvement in leaky negative capacitance fets," *IEEE Electron Device Letters*, vol. 38, no. 9, pp. 1335–1338, 2017. doi: 10.1109/LED.2017.2733382
- <sup>25</sup> A. I. Khan, U. Radhakrishna, K. Chatterjee, S. Salahuddin, and D. A. Antoniadis, "Negative capacitance behavior in a leaky ferroelectric," *IEEE Transactions on Electron Devices*, vol. 63, no. 11, pp. 4416–4422, 2016.
- <sup>26</sup> A. Palma, A. Godoy, J. A. Jiménez-Tejada, J. E. Carceller, and J. A. López-Villanueva, "Quantum two-dimensional calculation of time constants of random telegraph signals in metal-oxide-semiconductor structures," *Phys. Rev. B*, vol. 56, pp. 9565–9574, 1997. doi: 10.1103/PhysRevB.56.9565. [Online]. Available: <https://link.aps.org/doi/10.1103/PhysRevB.56.9565>
- <sup>27</sup> F. Jiménez-Molinos, F. Gámiz, A. Palma, P. Cartujo, and J. A. López-Villanueva, "Direct and trap-assisted elastic tunneling through ultrathin gate oxides," *Journal of Applied Physics*, vol. 91, no. 8, pp. 5116–5124, 2002. doi: 10.1063/1.1461062
- <sup>28</sup> B. Sören, G. Julie, L. Gwendal, X. Bin, L. Nicolas, F. Stéphane, G. Stéphanie, C. Cécile, G. Karin, X. Stéphane, T. Jean, B. Laurent, B. Manuel, B. Agnès, S. Sylvain, and G. Vincent, "Learning through ferroelectric domain dynamics in solid-state synapses," *Nature Communications*, vol. 8, 2017. doi: 10.1038/ncomms14736
- <sup>29</sup> B. C.-m. Lai, "Leakage Current Mechanism of Metal-Ta<sub>2</sub>O<sub>5</sub>-Metal Capacitors for Memory Device Applications," *Journal of The Electrochemical Society*, vol. 146, p. 266, 1999. doi: 10.1149/1.1391597. [Online]. Available: <http://doi.org/10.1149/1.1391597>